INTERNATIONAL JOURNAL FOR NUMERICAL METHODS IN FLUIDS, VOL. 13, 235–250 (1991)

SOLUTION OF THE 3D LINEAR HYDRODYNAMIC EQUATIONS USING AN ENHANCED EIGENFUNCTION APPROACH

ALAN M. DAVIES

Proudman Oceanographic Laboratory, Bidston Observatory, Birkenhead, Merseyside LA43 7RA, U.K.

SUMMARY

A method is presented for solving the 3D hydrodynamic equations in homogeneous sea regions using the Galerkin approach in the vertical with a mixed basis set. The basis set is composed of eigenfunctions of the eddy viscosity profile and a fixed function through the vertical, the amplitude of which is related to the externally applied surface wind stress. By this means the high-shear near-surface layer, which has previously been difficult to resolve using eigenfunction expansions, is accurately represented in the solution.

The computational advantages of this approach compared with other basis functions, in terms of computer time and memory, and the ease of implementation on parallel processors with vector facilities are briefly discussed.

The accuracy of the method and the choice of the additional function is demonstrated for the problem of wind-induced currents in a rectangular sea region.

Calculations clearly show that for wind-induced currents this new approach is significantly more accurate than the 'classical' eigenfunction method. Also, the new method retains the advantages of the eigenfunction approach, namely insight into the mechanisms involved and ease of implementation on vector–parallel computers, together with minimization of computer time and memory.

1. INTRODUCTION

Solution of the three-dimensional hydrodynamic equations for tidal and wind-driven flows using the Galerkin approach with a set of functions (the basis set) in the vertical has proved a valuable alternative to using finite difference methods.[1–6]

A range of basis functions have been used, namely Legendre polynomials,[7,8] Chebyshev polynomials[9] and eigenfunctions.[1,10,11] The computational advantages of eigenfunctions in terms of minimizing the computational effort[12] and their ideal nature for parallel processing on multiprocessor vector computers[13,14] have recently been reported.

Although a basis set of eigenfunctions is ideal for tidal problems and has been used very successfully in an extensive number of applications,[2,3,11,15] a basis set of these functions is not ideal for wind-driven problems. For these problems, calculations[1,2] show that the rate of convergence of the eigenfunction expansion in the near-surface layer is slow. The basic reason for this is that the vertical derivative of the eigenfunction is usually taken as zero at the surface (an ideal boundary condition for tides); however, when a wind stress is applied, the expansion is found to converge extremely slowly in the near-surface layer. An enhanced rate of convergence can be obtained by generating eigenfunctions which are sheared in the near-surface layer (a 'sheared

0271–2091/91/120235–16$08.00

Received March 1990
Revised August 1990

eigenfunction' approach[16]), although in this case Davies[16] found that additional terms were generated which coupled the hydrodynamic equations. This increased the computational overhead, and also the coupling meant that the algorithm was not suitable for parallel processing.

In this paper an alternative approach is presented in which a mixed basis set is used, composed of a single, fixed, specified function through the vertical, the magnitude of which is proportional to the wind stress, and the classical expansion of eigenfunctions having a zero derivative at the surface.[10] This new method we will refer to in this paper as an 'enhanced eigenfunction' approach.

The purpose of the specified function is to accurately represent the surface shear layer, leaving a smoother solution which can be readily approximated with a small number of eigenfunctions. The method is similar to the tau approach.[17] It has the computational advantage over the 'sheared eigenfunction' method[16] of yielding an uncoupled set of equations (in the case of the linear hydrodynamic equations) but retaining a high rate of convergence.

The mathematical development of the method is presented in the next section, with subsequent sections examining the rate of convergence for wind-driven currents in a closed rectangular basin. In order to compare the rates of convergence of the new approach with the 'classical' method,[1,2,5,10] the rectangular basin is chosen to approximate the North Sea with identical dimensions to those used by these other authors.

2. SOLUTION OF THE HYDRODYNAMIC EQUATIONS

2.1. Three-dimensional equations

Here for the sake of clarity we consider the linear hydrodynamic equations in Cartesian co-ordinates, although the method can be readily extended to the non-linear equations (see Reference 18 for the solution of these equations using the Galerkin approach) or to polar co-ordinates.[2]

The working equations in sigma co-ordinates, $\sigma = z/h$, are given by

$$\frac{\partial \zeta}{\partial t} + \frac{\partial}{\partial x}\left(h\int_0^1 u\,\mathrm{d}\sigma\right) + \frac{\partial}{\partial y}\left(h\int_0^1 v\,\mathrm{d}\sigma\right) = 0, \tag{1}$$

$$\frac{\partial u}{\partial t} - \gamma v = -g\frac{\partial \zeta}{\partial x} + \frac{1}{h^2}\frac{\partial}{\partial \sigma}\left(\mu\frac{\partial u}{\partial \sigma}\right), \tag{2}$$

$$\frac{\partial v}{\partial t} + \gamma u = -g\frac{\partial \zeta}{\partial y} + \frac{1}{h^2}\frac{\partial}{\partial \sigma}\left(\mu\frac{\partial v}{\partial \sigma}\right). \tag{3}$$

In these equations, t denotes time, x, y and z are Cartesian co-ordinates and u, v are the x- and y-components of velocity respectively. The acceleration due to gravity, g, and the geostrophic coefficient γ are taken as constant, with μ the vertical eddy viscosity and h the water depth.

The surface and bed boundary conditions in sigma co-ordinates are given by

$$-\rho\left(\frac{\mu}{h}\frac{\partial u}{\partial \sigma}\right)_0 = F_S, \qquad -\rho\left(\frac{\mu}{h}\frac{\partial v}{\partial \sigma}\right)_0 = G_S, \tag{4}$$

$$-\rho\left(\frac{\mu}{h}\frac{\partial u}{\partial \sigma}\right)_1 = F_B, \qquad -\rho\left(\frac{\mu}{h}\frac{\partial v}{\partial \sigma}\right)_1 = G_B. \tag{5}$$

In these equations, ρ is the density, F_S and G_S are the x- and y-components of surface wind stress respectively and F_B and G_B are the x- and y-components of bed stress respectively.

2.2. *Numerical solution*

Here we briefly outline the major steps in solving equations (1)–(3) using the Galerkin approach with the 'enhanced' eigenfunction method.

Consider initially the u- and v-components of current expressed as

$$U=\psi_u+U_p, \qquad V=\psi_v+V_p, \tag{6}$$

with U_p and V_p approximated by expansion.

$$U_p=\sum_{r=1}^{m} A_r f_r(\sigma), \qquad V_p=\sum_{r=1}^{m} B_r f_r(\sigma), \tag{7}$$

where $\psi_u(x, y, z, t)$ and $\psi_v(x, y, z, t)$ are specified external functions and U_p and V_p are expanded in terms of m basis functions $f_r(\sigma)$ and coefficients $A_r(x, y, t)$ and $B_r(x, y, t)$ respectively.

Substituting expansions (6) in equation (1) gives

$$\frac{\partial\zeta}{\partial t}=-\frac{\partial}{\partial x}\left(h\int_0^1 U_p\mathrm{d}\sigma\right)-\frac{\partial}{\partial y}\left(h\int_0^1 V_p\mathrm{d}\sigma\right)-\frac{\partial}{\partial x}\left(h\int_0^1 \psi_u\mathrm{d}\sigma\right)-\frac{\partial}{\partial y}\left(h\int_0^1 \psi_v\mathrm{d}\sigma\right). \tag{8}$$

Applying the Galerkin method to the solution of equation (2), multiplying by f_r and integrating from sea surface to sea bed, with the term involving viscosity being integrated by parts (see References 1 and 2 for details), gives, after some rearranging and insertion of surface and bed boundary conditions (4) and (5),

$$\int_0^1 \frac{\partial U_p}{\partial t}f_r\mathrm{d}\sigma=\gamma\int_0^1 V_p f_r\mathrm{d}\sigma-g\frac{\partial\zeta}{\partial x}\int_0^1 f_r\mathrm{d}\sigma-\frac{F_B}{\rho h}f_r(1)+\frac{F_S}{\rho h}f_r(0)-\frac{1}{h^2}\int_0^1 \mu\frac{\partial U_p}{\partial\sigma}\frac{\mathrm{d}f_r}{\mathrm{d}\sigma}\mathrm{d}\sigma+F_e, \tag{9}$$

where

$$F_e=-\int_0^1 \frac{\partial\psi_u}{\partial t}f_r\mathrm{d}\sigma+\gamma\int_0^1 \psi_v f_r\mathrm{d}\sigma-\frac{1}{h^2}\int_0^1 \mu\frac{\partial\psi_u}{\partial\sigma}\frac{\mathrm{d}f_r}{\mathrm{d}\sigma}\mathrm{d}\sigma. \tag{10}$$

2.3. *Form of basis functions*

The choice of basis functions f_r is arbitrary. The various computational advantages/disadvantages of using polynomials or eigenfunctions of the eddy viscosity distribution have been reported in the literature.[2,9,12] Calculations[19] showed that eigenfunctions could accurately represent high-shear near-bed layers when applied with a no-slip condition. However, in the case of wind-induced flow they converged slowly in the near-surface layer. This slow convergence is a direct result of the vertical derivative of the eigenfunction being zero at the surface.

In order to compare the present approach, in which functions ψ_u and ψ_v are added to the expansion, with the previous method of Heaps,[10] we chose the basis functions f_r to be eigenvalues of

$$\frac{\mathrm{d}}{\mathrm{d}\sigma}\left(\mu\frac{\mathrm{d}f}{\mathrm{d}\sigma}\right)=\varepsilon f, \tag{11}$$

subject to the surface boundary condition

$$\left.\frac{\mathrm{d}f}{\mathrm{d}\sigma}\right|_0=0. \tag{12}$$

Also, to be consistent with Heaps and to clearly determine the influence of ψ_u and ψ_v on the surface current, we also chose to solve the equations subject to a linear slip bottom boundary condition,[10] namely

$$-\rho\left(\frac{\mu}{h}\frac{\partial u}{\partial \sigma}\right)_1 = F_B = kpU_h, \qquad -\rho\left(\frac{\mu}{h}\frac{\partial v}{\partial \sigma}\right)_1 = G_B = kpV_h, \tag{13}$$

with k a linear friction coefficient.

Consider initially the u-component of velocity. Substituting equation (6) in (13) and separating into two equations gives

$$-\frac{\mu}{h}\frac{\partial \psi_u}{\partial \sigma}\bigg|_1 = k\psi_u(1), \tag{14}$$

$$-\frac{\mu}{h}\frac{\partial U_p}{\partial \sigma}\bigg|_1 = kU_p(1) \tag{15}$$

In order to satisfy (15) for arbitrary coefficients A_r in expansion (7), the eigenvalue problem (11) must be solved subject to the sea bed boundary condition

$$-\frac{\mu}{h}\frac{\mathrm{d}f_r}{\mathrm{d}\sigma}\bigg|_1 = kf_r(1). \tag{16}$$

In practice, since the bottom boundary condition is a natural boundary condition, it is not necessary for the eigenfunctions to satisfy it exactly. However, because our primary aim here is to compare the rate of convergence of the present 'enhanced' eigenfunction approach with the 'classical' method of Heaps,[10] we will compute eigenfunctions which solve (16) exactly.

Calculation of the eigenfunctions and eigenvalues of (11) can be readily accomplished for an arbitrary vertical variation of eddy viscosity using the Galerkin approach. Multiplying (11) by f_k and integrating the viscosity term by parts yields

$$\mu\frac{\mathrm{d}f_r}{\mathrm{d}\sigma}f_k\bigg|_1 - \mu\frac{\mathrm{d}f_r}{\mathrm{d}\sigma}f_k\bigg|_0 - \int_0^1 \mu\frac{\mathrm{d}f_r}{\mathrm{d}\sigma}\frac{\mathrm{d}f_k}{\mathrm{d}\sigma}\mathrm{d}\sigma = -\varepsilon_r\int_0^1 f_r f_k \mathrm{d}\sigma. \tag{17}$$

Equation (17) can be readily solved for an arbitrary vertical profile of eddy viscosity using standard numerical methods (e.g. Reference 1).

To be consistent with Heaps,[10] eigenfunctions and eigenvalues were obtained from equation (17) subject to boundary conditions (12) and (16).

Substituting (7) in (9) and using a basis set of orthogonal eigenfunctions normalized such that $f_r(0) = 1$, we obtain

$$\frac{\partial A_r}{\partial t}\int_0^1 f_r f_r \mathrm{d}\sigma = \gamma B_r \int_0^1 f_r f_r \mathrm{d}\sigma - g\frac{\partial \zeta}{\partial x}\int_0^1 f_r \mathrm{d}\sigma - \frac{F_B}{\rho h}f_r(1) + \frac{F_S}{\rho h}f_r(0)$$
$$-\frac{A_r\varepsilon_r}{h^2}\int_0^1 f_r f_r \mathrm{d}\sigma - \frac{\mu}{h^2}\sum_{j=1}^{m} A_j\frac{\mathrm{d}f_j}{\mathrm{d}\sigma}f_r + F_e. \tag{18}$$

In deriving (18) it is assumed that the eigenfunctions satisfy surface boundary condition (12), although no assumption has been made about the bottom boundary condition.

For the case in which the eigenfunctions have been computed subject to bottom boundary condition (16), equation (18) can be further simplified.

Using (15), (16) and expansion (7) we have

$$-\frac{\mu}{h^2}\sum_{j=1}^{m} A_j \frac{\mathrm{d}f_j}{\mathrm{d}\sigma} f_r\Big|_1 = \frac{k}{h} U_p(1) f_r(1). \tag{19}$$

Also, from (13) and (6) we have

$$\frac{F_B}{\rho h} = \frac{k}{h} U_p(1) + \frac{k}{\rho}\psi_u(1). \tag{20}$$

By substituting (19) and (20) in (18), the term involving the bottom stress F_B can be eliminated to give

$$\frac{\partial A_r}{\partial t}\int_0^1 f_r f_r \mathrm{d}\sigma = \gamma B_r \int_0^1 f_r f_r \mathrm{d}\sigma - g\frac{\partial \zeta}{\partial x}\int_0^1 f_r \mathrm{d}\sigma + \frac{F_S}{\rho h} f_r(0) - \frac{A_r \varepsilon_r}{h^2}\int_0^1 f_r f_r \mathrm{d}\sigma + \bar{F}_e, \tag{21}$$

where

$$\bar{F}_e = -\frac{k}{\rho}\psi_u(1) f_r(1) - \int_0^1 \frac{\partial \psi_u}{\partial t} f_r \mathrm{d}\sigma + \gamma \int_0^1 \psi_v f_r \mathrm{d}\sigma - \frac{1}{h^2}\int_0^1 \mu \frac{\partial \psi_u}{\partial \sigma}\frac{\mathrm{d}f_r}{\mathrm{d}\sigma}\mathrm{d}\sigma. \tag{22}$$

To be consistent with Heaps,[10] it is convenient to express coefficients A_r and B_r as

$$A_r = U_r \Phi_r, \qquad B_r = V_r \Phi_r,$$

giving, from equation (8),

$$\frac{\partial \zeta}{\partial t} = -\frac{\partial}{\partial x}\left(h\sum_{r=1}^{m} u_r \Phi_r a_r\right) - \frac{\partial}{\partial y}\left(h\sum_{r=1}^{m} v_r \Phi_r a_r\right) + H_e, \tag{23}$$

where

$$H_e = -\frac{\partial}{\partial x}\left(h\int_0^1 \psi_u \mathrm{d}\sigma\right) - \frac{\partial}{\partial y}\left(h\int_0^1 \psi_v \mathrm{d}\sigma\right), \qquad a_r = \int_0^1 f_r \mathrm{d}\sigma.$$

From equation (21) we have

$$\frac{\partial U_r}{\partial t} = \gamma V_r - g\frac{\partial \zeta}{\partial x} a_r + \frac{F_S}{\rho h} f_r(0) - \frac{U_r \varepsilon_r}{h^2} + \bar{F}_e, \tag{24}$$

with $\bar{F}_e$ given by (22).

In an analogous manner a similar equation for the v-current can be obtained.

Comparing equations (23) and (24), derived using the Galerkin method with a basis of eigenfunctions satisfying a slip bottom boundary condition, with the corresponding equations obtained by Heaps[10] shows the equations to be identical except for the additional terms H_e and $\bar{F}_e$. These terms arise due to the additional functions ψ_u and ψ_v in expansions (6).

The first five of these eigenfunctions computed with μ constant at $0{\cdot}0130\ \mathrm{m^2\,s^{-1}}$ and $k = 0{\cdot}002\ \mathrm{m\,s^{-1}}$ are shown in Figure 1. It is clear from this figure that the modes are sheared in the near-bed layer, a consequence of satisfying exactly the bottom slip boundary conditions. However, they have a zero vertical derivative at the surface, owing to boundary condition (12), and we will show this leads to a slow rate of convergence in the surface layer.

Obviously, if the terms ψ_u and ψ_v can be chosen to improve the rate of convergence of the eigenfunction expansion in the near-surface layer during wind forcing (a situation where the 'classical' eigenfunction approach proved inaccurate[1,2]), then the present method yielding a set of

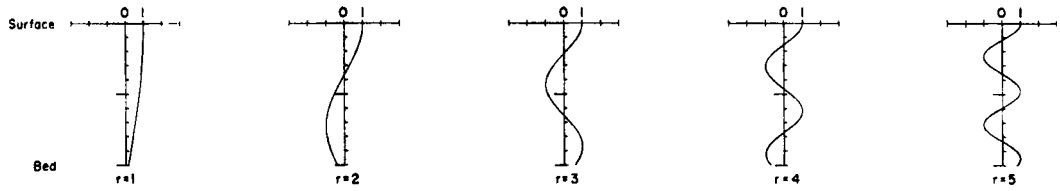

Figure 1. Vertical profiles of the first five modes computed with $\mu = 0{\cdot}0130\ \mathrm{m^2\,s^{-1}}$ and $k = 0{\cdot}002\ \mathrm{m\,s^{-1}}$

m uncoupled equations will have advantages over the 'classical' eigenfunction approach of Heaps.[10] The choice of ψ_u and ψ_v is considered in the next section.

2.4. *Initial conditions*

The coefficients A_r and B_r in equation (7) can be readily determined at the start of a calculation (time $t=0$) from a knowledge of the initial specified flow fields $U(0)$ and $V(0)$. Hence, substituting (7) in (6) at time $t=0$, we have

$$U(0)=\psi_u+\sum_{r=1}^{m} A_r(0)f_r(\sigma), \qquad V(0)=\psi_v+\sum_{r=1}^{m} B_r(0)f_r(\sigma), \tag{25}$$

with $A_r(0)$ and $B_r(0)$ the coefficients at time $t=0$. Rearranging (25) and using the orthogonality property of the eigenfunctions gives

$$A_r(0)=\left(\int_0^1 U(0)f_r(\sigma)-\int_0^1 \psi_u f_r(\sigma)\right)\Big/\int_0^1 f_r^2(\sigma)\mathrm{d}\sigma, \tag{26}$$

with B_r determined in an analogous manner. In many probelms the initial flow fields $U(0)$ and $V(0)$ are zero, leading to a further simplification of (26). The integrals in (26) can be readily computed by numerical means.

It is important to note that the computation of the coefficients $A_r(0)$ and $B_r(0)$ in (26) with zero initial flow fields is different than in the 'classical' approach where the initial condition is satisfied exactly, irrespective of the number of terms, m, in expansion (25), by setting the coefficients to zero. In the 'enhanced convergence' approach with ψ_u and ψ_v non-zero in (25) the initial conditions can only be approximated for a finite m and this could have some effect upon the accuracy of a short-time integration for m small. However, as we will show in a subsequent section, this did not appear to be a major problem.

3. CHOICE OF ENHANCEMENT FUNCTIONS ψ_u AND ψ_v

Previous calculations[1,2,19] have clearly shown that eigenfunctions, are ideal for tides but have a low rate of convergence for wind-driven problems, i.e. problems where the surface stress is non-zero. Using this fact, it is sensible for ψ_u and ψ_v to be of the form

$$\psi_u=\frac{hF_S}{\rho\mu(0)}\beta\psi(\sigma), \tag{27}$$

$$\psi_v=\frac{hG_S}{\rho\mu(0)}\beta\psi(\sigma), \tag{28}$$

with ψ_u and ψ_v proportional to the wind stress and where the factor $\beta h/\rho\mu(0)$, with β a free

parameter, is used with $\psi(\sigma)$, a function in the vertical, to determine both the profiles of ψ_u and ψ_v and their vertical derivatives.

Heaps[10] showed that in the case of constant eddy viscosity the truncation error in expansion (7) after m terms would be approximated by ψ_u and ψ_v with $\beta=1$ and

$$\psi(\sigma)=\frac{2}{\pi^2}\left[(3\sigma^2-6\sigma+2)\frac{\pi^2}{12}-\sum_{r=1}^{m-1}\cos\left(\frac{r\pi\sigma}{r^2}\right)\right] \quad \text{(function 1)}. \tag{29}$$

Substituting (29) in (27) and (28) and computing $\partial\psi/\partial\sigma$ at the surface, it is evident that for $\beta=1$, ψ_u and ψ_v satisfy exactly the surface stress boundary condition.

An alternative to (29) is

$$\psi(\sigma)=\frac{\mu_0 h}{k}\left(1-\frac{kh}{\mu_0}(\sigma-1)\right) \quad \text{(function 2)}. \tag{30}$$

Again in the case of $\beta=1$ the surface stress boundary condition can be satisfied exactly. Also, bottom linear slip boundary conditions (13) are satisfied by (30). However, in the case in which the more physically realistic quadratic friction law is applied at the sea bed, or modes satisfying a no-slip bottom boundary condition are applied, this could be a restriction.

Although in this paper we are primarily concerned with comparing the present approach with that of Heaps[10] using a slip condition, it is advantageous to consider other types of functions than those given by equations (29) and (30). Calculations have shown that the Galerkin approach can be readily applied with quadratic friction and also a no-slip bottom boundary condition. Bearing in mind these considerations, we also consider here a discontinuous form of $\psi(\sigma)$, namely

$$\psi(\sigma)=\begin{cases}(1/s)(\sigma^2/2-s\sigma+s^2/2), & \sigma<s\\ 0, & \sigma\geqslant s\end{cases} \quad \text{(function 3)}. \tag{31}$$

Again for $\beta=1$ this piecewise function satisfies the surface boundary condition. However, at $s=\sigma$ both its value and its derivative fall to zero, and below this value of σ the function vanishes.

Such a piecewise function is useful in that it can account for the near-surface shear layer, without influencing the solution below that layer, where previous calculations have shown that the eigenfunction expansion converges rapidly. The influence of the choice of the functional form of $\psi(\sigma)$ upon the rate of convergence of the various expansions will be considered in detail in the next section.

4. WIND-DRIVEN CURRENTS IN AN IDEALIZED NORTH SEA BASIN

4.1. Model description

To be consistent with previous calculations of Heaps[10] and other calculations using a range of polynomial functions or grid boxes in the vertical, we consider a closed rectangular North Sea basin ('the Heaps rectangle') having dimensions 400 km in the x-direction and 800 km in the y-direction. A uniform staggered grid (Arakawa C grid) was used in the horizontal with grid spacings $\Delta x=400/9$ km and $\Delta y=800/17$ km (see Reference 1 for details of the model). The sea, initially at rest, was subjected to a suddenly imposed and maintained wind stress, with values $F_S=0$ and $G_S=-1{\cdot}5\ \mathrm{N\,m^{-2}}$. A linear slip coefficient $k=0{\cdot}002\ \mathrm{m\,s^{-1}}$ was used in the calculation, with $\rho=1025\ \mathrm{kg\,m^{-3}}$, $g=9{\cdot}81\ \mathrm{m\,s^{-2}}$, Coriolis parameter $\gamma=1{\cdot}2\times10^{-4}\ \mathrm{s^{-1}}$ and water depth $h=65$ m. The unconditional time-stepping algorithm given in Reference 2 was used to integrate the equations, with a time step of 6 min.

In computing the Coriolis term on a staggered grid, it is necessary to average over four neighbouring velocity points. This procedure was used in the interior of the rectangle, although at points adjacent to the land only grid points in the sea region were used, the so-called 'wet points only' method of Jamart and Ozer.[5] This averaging method is slightly different from that of Heaps,[10] who used an average over four grid points everywhere, giving rise to a 'spurious' residual boundary layer current.[5]

4.2. Numerical calculations

4.2.1. Profiles 30 h after the onset of the wind. In order to compare the currents computed with the 'enhanced' eigenfunction method with previous calculations,[1,9,10,12] the eddy viscosity was fixed at $0{\cdot}0650\ m^2\ s^{-1}$ with the bottom friction coefficient $k = 0{\cdot}002\ m\ s^{-1}$. Surface and bottom currents at the centre of the basin, 30 h after the onset of the wind field, computed using the 'classical' eigenfunction method and the 'enhanced' eigenfunction method with the various functions given in equations (29)–(31), are shown in Table I.

Table I. U- and V-components of surface (S) and bottom (B) currents ($cm\ s^{-1}$) at the centre of the North Sea rectangle, 30 h after the imposition of the wind field, computed with an eddy viscosity of $650\ cm^2\ s^{-1}$, $\beta = 1$ and $s = 0{\cdot}25$

	Number of terms (m) in expansion			
	6	10	20	30
	No additional function			
U_S	−15·03	−15·06	−15·07	−15·07
V_S	−29·92	−32·14	−33·73	−34·25
U_B	7·13	7·12	7·12	7·12
V_B	11·38	11·09	10·97	10·95
	m			
	2	4	6	10
	Function 1			
U_S	−13·71	−14·91	−15·03	−15·07
V_S	−36·34	−35·34	−35·27	−35·24
U_B	7·80	7·17	7·13	7·12
V_B	8·55	10·65	10·85	10·90
	Function 2			
U_S	−13·72	−14·91	−15·03	−15·07
V_S	−35·72	−35·28	−35·26	−35·25
U_B	7·81	7·17	7·13	7·12
V_B	10·30	10·87	10·92	10·93
	Function 3			
U_S	−13·74	−14·91	−15·02	−15·06
V_S	−31·57	−35·65	−35·39	−35·21
U_B	7·82	7·17	7·13	7·12
V_B	13·16	10·95	10·81	10·95

It is evident from this table and from Figure 2 that the eigenfunction expansion for the u-component of current (the component at right angles to the wind direction) converges very rapidly. The surface boundary condition for this component is one of zero external stress, a boundary condition satisfied by each mode. However, in the case of the v-component of current (the component in the wind direction) the 'classical' eigenfunction expansion converges slowly, with 30 functions still not giving a fully converged solution (see Table I). Also, the v-component of current computed with $m=6$ shows significant 'ripples' in the vertical, which only disappear when $m=30$ (see Figure 2).

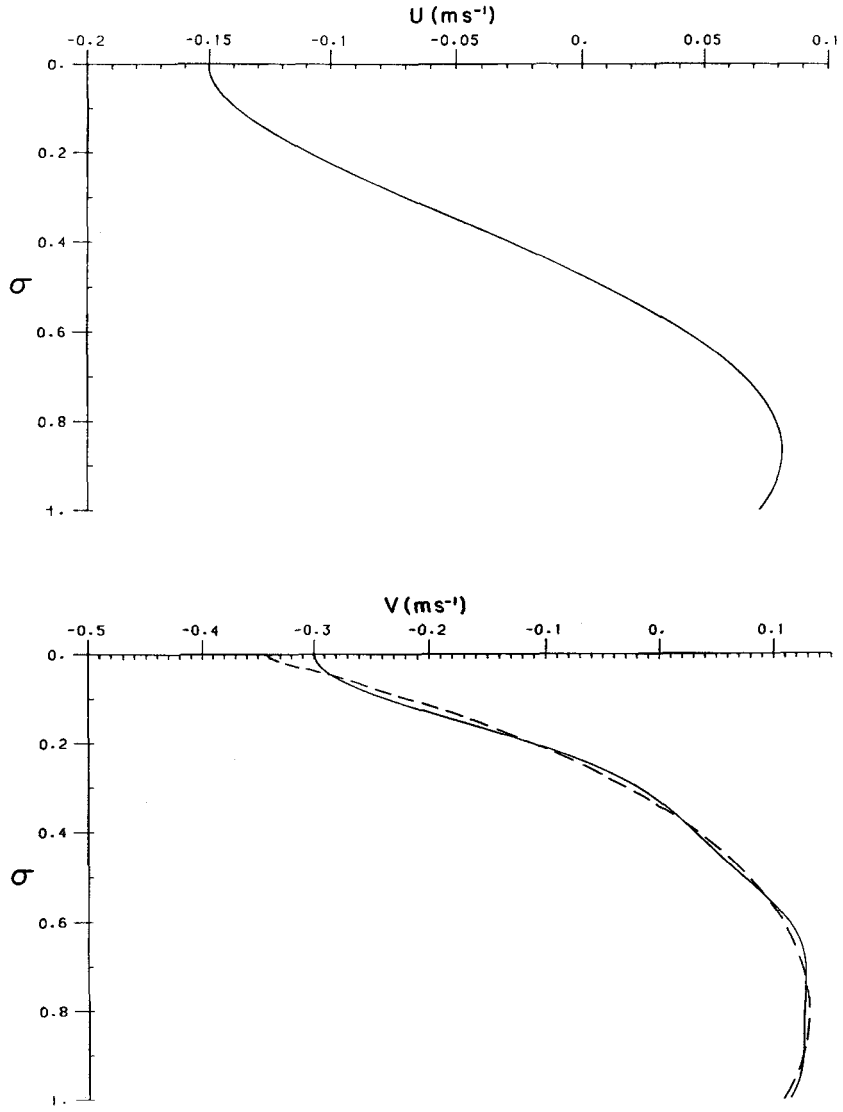

Figure 2. Velocity profiles (u- and v-components) at the centre of the basin, 30 h after the onset of the wind field, computed using $\mu=0{\cdot}0650\ \mathrm{m^2\,s^{-1}}$ with $m=6$ (——) and $m=30$ (– – –) by the 'classical' eigenfunction approach

In the case of the 'enhanced' eigenfunction approach the series converges very rapidly, irrespective of whether function 1, 2 or 3 (equations (29)–(31)) is used to enhance the rate of convergence, with maximum differences only of the order of 1% occurring in the surface v-component of current between solutions using $m=4$ and 10 functions (see Table I and Figure 3). Also from Table I it is evident that the surface current computed with $m=4$ using the 'enhanced' eigenfunction approach is significantly more accurate than that computed using the 'classical' approach with $m=30$.

It is apparent from Figure 3 that smooth profiles are computed using function 3 with $m=4$ (similar profiles were found with functions 1 and 2), which do not exhibit any of the 'ripples' found

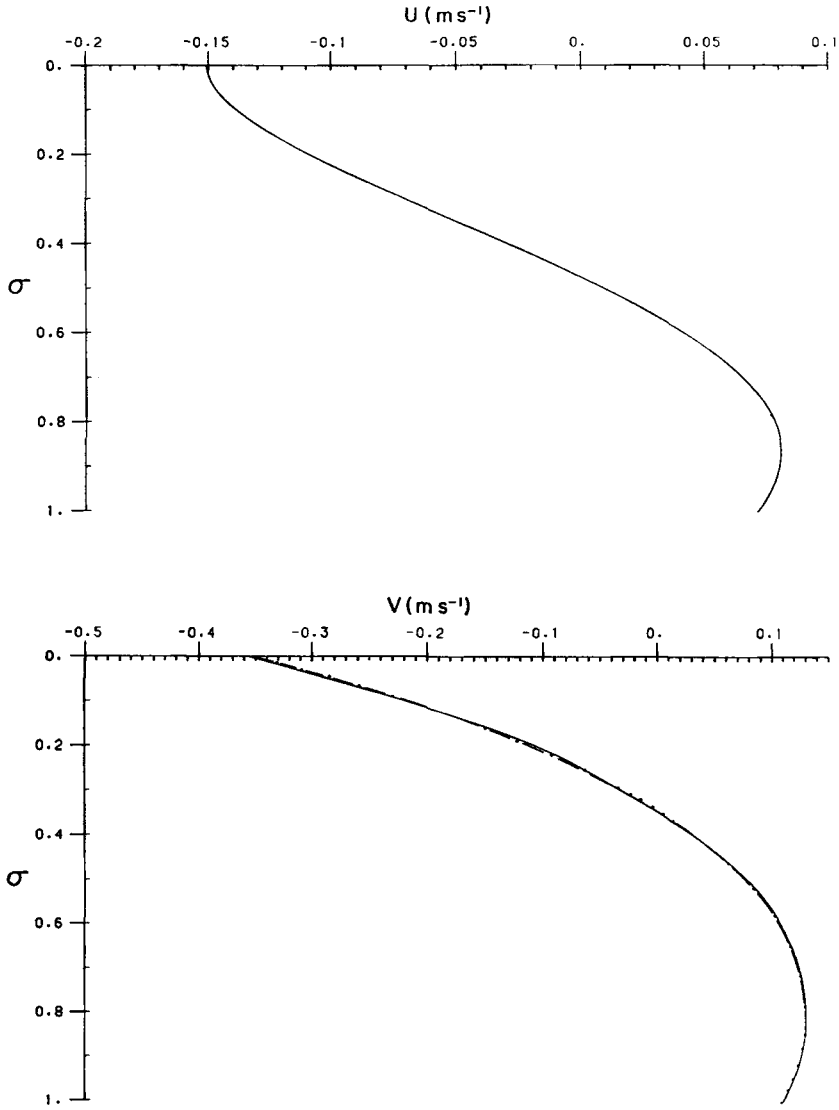

Figure 3. Velocity profiles (u- and v-components) at the centre of the basin, 30 h after the onset of the wind field, computed using $\mu=0{\cdot}0650\ \mathrm{m^2\,s^{-1}}$ with $m=4$ (——) and $m=10$ (– – –) by the 'enhanced' eigenfunction approach (function 3). Also shown are profiles computed with $m=30$ (····) by the 'classical' eigenfunction approach

previously (Figure 2) using the 'classical' eigenfunction approach with $m=6$. Certainly, current profiles using the 'enhanced' eigenfunction method are significantly smoother (Figure 3) than those computed using the 'classical' method, where ripples occur due to a Gibbs-type phenomenon associated with the expansion of eigenfunctions trying to fit the high-shear surface region. In the 'enhanced' method this region is accounted for by the external function, leaving a more smoothly varying solution which can be readily approximated by the eigenfunctions.

Comparing currents computed here with previous calculations using polynomial basis sets[9] or grid box methods,[12] it is clear that the present method is of comparable accuracy whilst retaining the low computational overhead (in terms of computer time and memory) of the eigenfunction approach compared to other methods.[12]

4.2.2. Profiles 3.5 h after the onset of the wind. In the previous series of calculations, profiles computed 30 h from the onset of the wind were compared with each other. The reason for choosing this specific time was that the rate of convergence and accuracy of the solution could be compared directly with previously published results. However, recent calculations using a point model in the vertical[2] have shown that the physical mechanism determining the current profile is an initial highly sheared surface layer, following the initial wind impulse, within which shear subsequently diminishes as the wind's momentum is transferred to depth. In these calculations the surface v-component of current reached a maximum about 3·5 h after the imposition of the wind. Consequently, a more rigorous test of the 'enhanced' eigenfunction approach is to examine the rate of convergence of the expansion at this time (Table II). Also, since this is a short-time integration, the influence of any inaccuracies in determining the initial conditions using the 'enhanced' eigenfunction method will be apparent. (Only surface and mid-depth currents are given in Table II, since bottom currents were small, of the order of a few $cm\,s^{-1}$ at this time.)

It is evident from Table II that, as expected, the 'classical' eigenfunction method again converges slowly in the case of the v-component of current. However, as in the previous calculation, the inclusion of one of the additional functions significantly enhances the rate of convergence, with an expansion of 10 functions showing little difference between current profiles computed using enhancement function 1, 2 or 3. It is apparent, however, from Table II (V-surface currents in particular) that the eigenfunction expansion appears to converge more rapidly using function 1 or 2 rather than 3. To examine this in more detail, the calculation was repeated with the eddy viscosity reduced by a factor of five to $0{\cdot}0130\ m^2\,s^{-1}$, giving significantly enhanced shear in the surface layer at time $t=3{\cdot}5$ h. It is evident from Table III that in this case the 'classical' eigenfunction method converges very slowly, with a significant difference in the surface v-component of current computed with $m=20$ or 30 (see Table III and Figure 4). As in the previous calculations, vertical 'ripples' due to a Gibbs-type effect are present even when m is increased to 20, and only with $m=30$ do they become negligible (Figure 4). (Only surface currents are shown in Table III, since currents below this layer were small and converged rapidly as m was increased.)

It is evident from Figure 5 and Table III that using the 'enhanced' eigenfunction approach (Calc. A) with $m=4$ (Figure 5) also yields some 'ripples' in this calculation. However, these 'ripples' are no longer present when m is increased to 10 (Figure 5), giving profiles as smooth as those computed using the 'classical' eigenfunction method with $m=30$ (compare Figures 4 and 5). No inaccuracies due to the approximation of the initial conditions using the 'enhanced' eigenfunction method were found in the calculations (see Table II, Calc. A and a comparison of Figures 4 and 5).

Again, currents computed using the 'enhanced' eigenfunction approach with $m=6$ or 10 terms in the expansion are not significantly different for the three functions considered here (see Table III, Calc. A), although it would appear that the rate of convergence is slightly faster with

Table II. U- and V-components of surface (S) and mid-depth (M) currents ($cm\,s^{-1}$) at the centre of the rectangular basin, 3·5 h after the imposition of the wind field, computed with an eddy viscosity of $650\,cm^2\,s^{-1}$, $\beta=1$ and $s=0{\cdot}25$

	Number of terms (m) in expansion			
	6	10	20	30
	No additional function			
U_S	−25·84	−25·87	−25·88	−25·88
V_S	−53·38	−55·63	−57·20	−57·73
U_M	−11·03	−11·02	−11·02	−11·02
V_M	−14·27	−13·94	−13·49	−13·78
	m			
	2	4	6	10
	Function 1			
U_S	−24·52	−25·72	−25·83	−25·87
V_S	−59·60	−58·80	−58·74	−58·71
U_M	−11·94	−10·97	−11·03	−11·02
V_M	−12·74	−13·85	−13·75	−13·77
	Function 2			
U_S	−24·52	−25·72	−25·84	−25·87
V_S	−58·91	−58·72	−58·72	−58·72
U_M	−11·94	−10·97	−11·03	−11·02
V_M	−13·55	−13·77	−13·77	−13·77
	Function 3			
U_S	−24·52	−25·72	−25·83	−25·87
V_S	−54·53	−59·11	−58·85	−58·68
U_M	−11·94	−10·97	−11·03	−11·02
V_M	−17·24	−13·64	−13·62	−13·80

function 2 than with function 1, which in turn is preferable to function 3. However, these differences are not that significant.

In calculations A the enhancement function ψ was chosen to satisfy the surface boundary condition. In the Galerkin approach this is not necessary and in a final series of calculations (Calc. B) the influence upon accuracy of not satisfying this boundary condition was investigated. To this end β was changed from 1 to 0·75, giving a surface stress for each 'enhancement function' which is 25% less than the applied stress. Also, in the case of function 3, s was set at 0·125.

As expected, it is clear from a comparison of calculations A and B in Table III that with $\beta=0{\cdot}75$ the series converges more slowly (although naturally faster than the 'classical' approach, equivalent to $\beta=0$). However, with $m=10$ the surface v-component of current is only of the order of 3% less than the true solution (taken to be $130\,cm\,s^{-1}$; Table III)—a solution significantly more accurate than that obtained using the 'classical' approach with $m=20$, giving an error of 12%.

Although the use of a low eddy viscosity value at these high wind speeds may be somewhat, artificial it does clearly demonstrate the computational advantages of the new method developed here.

Table III. U- and V-components of surface (S) current ($cm\,s^{-1}$) at the the centre of the rectangular basin, 3·5 h after the imposition of the wind field, computed with an eddy viscosity of 130 $cm^2\,s^{-1}$, initially with $\beta=1$ and $s=0{\cdot}25$ and subsequently with $\beta=0{\cdot}75$ and $s=0{\cdot}125$ (Calc. B)

		Number of terms (m) in expansion			
		6	10	20	30
		No additonal function			
	U_S	−62·56	−63·35	−63·54	−63·55
	V_S	−104·07	−114·70	−122·54	−125·10
		m			
Calc.		2	4	6	10
		Function 1			
A	U_S	−46·62	−60·23	−62·56	−63·34
	V_S	−146·69	−131·68	−130·52	−130·12
B	U_S	−46·62	−60·23	−62·56	−63·34
	V_S	−125·19	−121·53	−123·91	−126·26
		Function 2			
A	U_S	−46·63	−60·23	−62·56	−63·35
	V_S	−139·84	−130·65	−130·19	−130·13
B	U_S	−46·63	−60·23	−62·56	−63·35
	V_S	−120·05	−120·75	−123·66	−126·27
		Function 3			
A	U_S	−46·62	−60·17	−62·48	−63·29
	V_S	−125·00	−132·71	−130·73	−129·96
B	U_S	−46·71	−60·43	−62·82	−63·63
	V_S	−89·88	−115·49	−124·11	−127·74

5. CONCLUDING REMARKS

It is clear from the mathematical analysis presented in Section 2 that by using the Galerkin approach with an expansion in terms of a fixed function ('enhancement' function, to approximate a wind-driven high-shear region) and a basis set of eigenfunctions, a more generalized eigenfunction method than that developed by Heaps[10] can be obtained. It is apparent that the present method can include time-varying wind stress and eddy viscosity. Also, the vertical variation of eddy viscosity is arbitrary, although a constant value has been used here to be consistent with Heaps.[10] Obviously, if the external function is omitted and the basis set is not chosen to be eigenfunctions, the present method is identical to that of References 1, 2 and 9.

It is clear from the calculations presented here that the 'enhanced' eigenfunction method converges more rapidly than the 'classical' approach. Also, it gives solutions of comparable accuracy to those obtained using other polynomial functions[9] or a grid box method[12] while retaining the major advantages of a set of uncoupled linear equations, which are ideal for solution on vector multiprocessor computers.[13,14]

It is clear from the calculations presented here that there is a significant advantage in ensuring that the 'enhancement' functions do satisfy the surface boundary condition in a wind stress problem. In this case it appears that the eigenfunction expansion converges slightly more rapidly

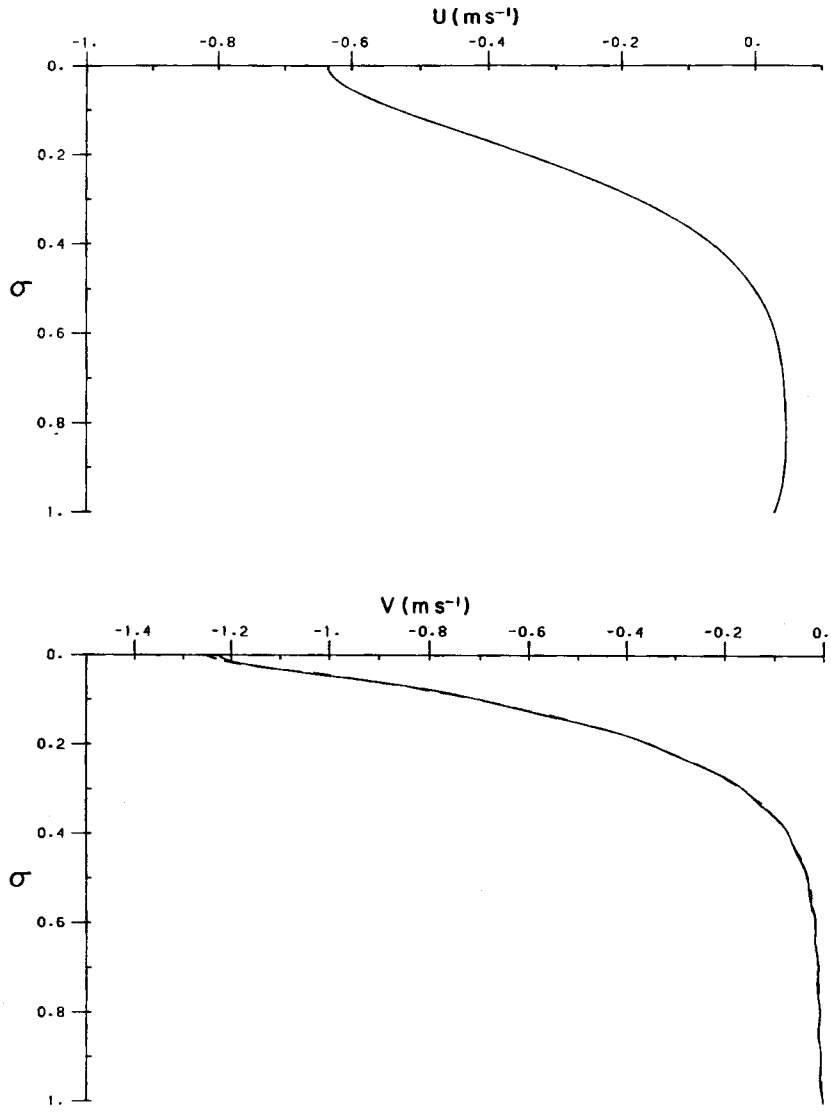

Figure 4. Velocity profiles (u- and v-components) at the centre of the basin, 3·5 h after the onset of the wind field, computed using $\mu = 0{\cdot}0130\ \mathrm{m^2\,s^{-1}}$ with $m = 20$ (——) and $m = 30$ (– – –) by the 'classical' eigenfunction approach

with function 2, satisfying exactly both surface and bottom boundary conditions, than with function 1, an analytic solution satisfying the surface boundary, which in turn converges more rapidly than function 3, chosen empirically. However, when the eddy viscosity is not constant in the vertical but exhibits a more physically realistic profile, or a quadratic bottom friction law is applied (again more physically realistic), then the analytic equivalents of functions 1 and 2 would not be available and function 3 or something equivalent would have to be used. Also, as shown in Table III, this function has some advantages if the surface boundary condition is not satisfied exactly.

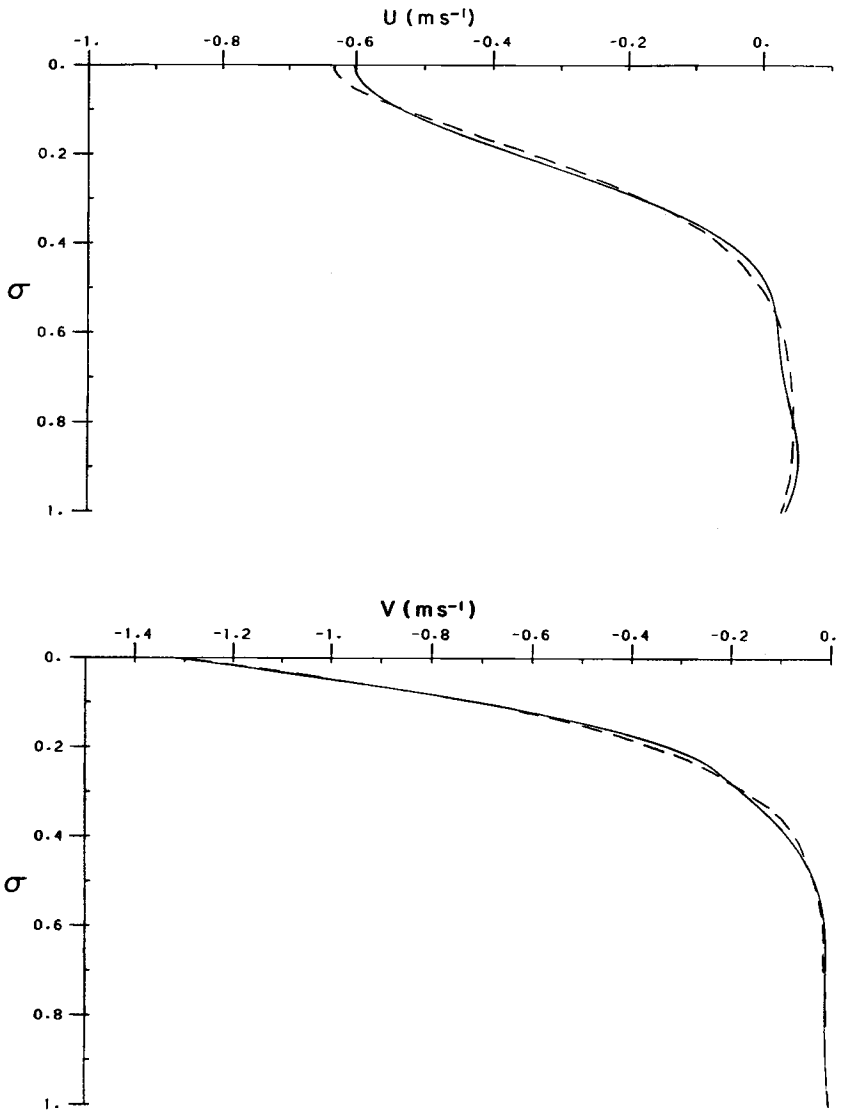

Figure 5. Velocity profiles (u- and v-components) at the centre of the basin, 3·5 h after the onset of the wind field, computed using $\mu = 0{\cdot}0130\ \mathrm{m^2\,s^{-1}}$ with $m = 4$ (——) and $m = 10$ (– – –) by the 'enhanced' eigenfunction approach (function 3)

Calculations are presently in progress using the method developed here to simulate three-dimensional time-varying wind-induced currents in a high-resolution fine-grid model of the Celtic and Irish Seas, and results will be reported subsequently.

ACKNOWLEDGEMENTS

The care taken by Mr. R. A. Smith in preparing the diagrams and Mrs. J. Hardcastle in typing the paper is very much appreciated.

REFERENCES

1. A. M. Davies, 'Formulation of a linear three-dimensional hydrodynamic sea model using a Galerkin–eigenfunction method', *Int. j. numer. methods fluids*, **3**, 33–60 (1983).
2. A. M. Davies, 'Spectral models in continental shelf sea oceanography', in N. S. Heaps (ed.), *Three-Dimensional Coastal Ocean Models*, AGU, Washington, U.S.A., 1987, pp. 71–106.
3. G. K. Furnes, 'A three dimensional numerical sea model with eddy viscosity varying piecewise linearly in the vertical', *Continental Shelf Res.*, **2**, 231–242 (1983).
4. R. B. Gordon and M. L. Spaulding, 'Numerical simulations of the tidal- and wind-driven circulation in Narragansett Bay', *Estuarine, Costal Shelf Sci.*, **24**, 611–636 (1987).
5. B. M. Jamart and J. Ozer, 'Numerical boundary layers and spurious residual flows', *J. Geophys. Res.*, **91**, 621–631 (1986).
6. M. L. Spaulding and T. Isaji, 'Three dimensional continental shelf hydrodynamic model including wave current interaction', in J. C. J. Nihoul and B. M. Jamart (eds), *Three-dimensional Models of Marine and Estuarine Dynamics*, Elsevier, Amsterdam, 1987, pp. 405–426.
7. A. Owen, 'A three-dimensional model of the Bristol Channel', *J. Phys. Oceanogr.*, **10**, 1290–1302 (1980).
8. M. L. Spaulding, T. Isaji, D. Mendelsohn and A. C. Turner, 'Numerical simulation of wind driven flow through the Bering Strait', *J. Phys. Oceanogr.*, **17**, 1799–1816 (1987).
9. A. M. Davies and A. Owen, 'Three-dimensional numerical sea model using the Galerkin method with a polynomial basis set', *Appl. Math. Modell.*, **3**, 421–428 (1979).
10. N. S. Heaps, 'On the numerical solution of the three dimensional hydrodynamical equations for tides and storm surges', *Mem. Soc. Sci. Liege Ser. 6*, **2**, 143–180 (1972).
11. N. S. Heaps and J. E. Jones, 'Three-dimensional model for tides and surges with vertical eddy viscosity prescribed in two layers—II. Irish Sea with bed friction layer', *Geophys. J. R. Astronon. Soc.*, **64**, 303–320 (1981).
12. A. M. Davies and C. V. Stephens, 'Comparison of the finite difference and Galerkin methods as applied to the solution of the hydrodynamic equations', *Appl. Math. Modell.*, **7**, 226–240 (1983).
13. A. M. Davies and R. Proctor, 'Developing and optimizing a 3D-spectral/finite difference hydrodynamic model for the CRAY X-MP', *Comput. Fluids*, **18**, 259–270 (1989).
14. A. M. Davies, R. B. Grzonka and C. V. Stephens, 'The implementation of hydrodynamic numerical sea models on the CRAY X-MP', *Advances in Parallel Computing*, **2** (to appear).
15. G. K. Furnes and M. Mork, 'Formulation of a continuously stratified sea model with three-dimensional representation of the upper layer', *Coastal Eng.*, **11**, 415–445 (1987).
16. A. M. Davies, 'Application of a Galerkin–eigenfunction method to computing currents in homogeneous and stratified seas', in K. W. Morton and M. J. Baines (eds), *Numerical Methods for Fluid Dynamics*, Academic Press, London, 1982, pp. 287–301.
17. D. Gottlieb and S. Orszag, 'A numerical analysis of spectral methods', *NSF–CBMS Monograph 26*, Society for Industrial and Applied Mathematics, Philadelphia, PA, 1977.
18. A. M. Davies, 'Application of the Galerkin method to the formulation of a three-dimensional non linear hydrodynamic sea model', *Appl. Math. Modell.*, **4**, 245–256 (1980).
19. A. M. Davies, 'On the accuracy of finite difference and spectral methods for computing tidal and wind wave current profiles', *Int. j. numer. methods. fluids*, **12**, 101–124 (1991).